Seasonal variation in the correlation between anomalies of sea level and chlorophyll in the Antarctic Circumpolar Current

Hajoon Song[1], Matthew C. Long[2], Peter Gaube[3], Ivy Frenger[4], John Marshall[5], Dennis J. McGillicuddy Jr.[6]

H. Song, hajsong@mit.edu

[1]Department of Atmospheric Sciences, Yonsei University, Seoul, Korea

[2]Climate and Global Dynamics Laboratory, National Center for Atmospheric Research, Boulder, Colorado, USA

[3]Applied Physics Laboratory, University of Washington, Seattle, Washington, USA

[4]GEOMAR Helmholtz Center for Ocean Research Kiel, Kiel, Germany

This article has been accepted for publication and undergone full peer review but has not been through the copyediting, typesetting, pagination and proofreading process, which may lead to differences between this version and the Version of Record. Please cite this article as doi: 10.1029/2017GL076246

The Antarctic Circumpolar Current (ACC) has highly energetic mesoscale phenomena, but their impacts on phytoplankton biomass, productivity, and biogeochemical cycling are not understood well. We analyze satellite observations and an eddy-rich ocean model to show that they drive chlorophyll anomalies of opposite sign in winter versus summer. In winter, deeper mixed layers in positive sea surface height (SSH) anomalies reduce light availability, leading to anomalously low chlorophyll concentrations. In summer with abundant light, however, positive SSH anomalies show elevated chlorophyll concentration due to higher iron level, and an iron budget analysis reveals that anomalously strong vertical mixing enhances iron supply to the mixed layer. Features with negative SSH anomalies exhibit the opposite tendencies: higher chlorophyll concentration in winter and lower in summer. Our results suggest that mesoscale modulation of iron supply, light availability and ver-

[5]Department of Earth, Atmospheric and Planetary Sciences, Massachusetts Institute of Technology, Cambridge, Massachusetts, USA

[6]Department of Applied Ocean Physics and Engineering, Woods Hole Oceanographic Institution, Woods Hole, Massachusetts, USA

tical mixing plays an important role in causing systematic variations in primary productivity over the seasonal cycle.

Keypoints:

- The correlation between anomalies of sea level and anomalies of chlorophyll has seasonality in the Antarctic Circumpolar Current.
- A positive correlation in summer results from the anomalous iron concentration that leads to chlorophyll anomalies.
- A negative correlation in winter results from the anomalous light level available for primary production.

1. Introduction

The ocean is rich in mesoscale phenomena that account for more than 90% of the kinetic energy in the surface ocean [*Ferrari and Wunsch*, 2009] and are known to play a critical role in transporting momentum, heat, and energy [*Robinson*, 1983; *Wunsch*, 1999; *Xu et al.*, 2014]. The mesoscale modulates marine ecosystems via effects on both the physical and chemical environment, influencing, for instance, nutrient supply, light levels and the diversity of phytoplankton populations [*McGillicuddy et al.*, 2007; *Rodríguez et al.*, 2001; *Clayton et al.*, 2016]. This modulation is clearly seen in chlorophyll concentrations (CHL). Anomalies of satellite CHL, a proxy for phytoplankton biomass, are observed to be correlated with sea surface height (SSH) anomalies, a proxy for mesoscale phenomena, in many regions of the ocean [*Chelton et al.*, 2011a; *Gaube et al.*, 2014]. Depending on the prevailing mechanisms, both positive and negative correlations between SSH and CHL ($\rho_{SSH',CHL'}$) can be expected. A wide range of mechanisms have been proposed by which the mesoscale modulates biogeochemistry, as reviewed in *McGillicuddy* [2016].

In situ and satellite observations have revealed mixed-layer depth (MLD) modulation by mesoscale dynamics; deeper (shallower) MLDs are associated with anticyclones (cyclones) with positive (negative) SSH anomalies in the subtropical ocean [*Gaube et al.*, 2013; *Dufois et al.*, 2014] and also in the Southern Ocean (SO) [*Hausmann et al.*, 2017]. While the influence of mesoscale dynamics on the MLD, nitrate, and CHL in the subtropical gyres has received some attention [*Dufois et al.*, 2014, 2016], these processes remain understudied in the SO, which is a region of major importance for biogeochemical cycling and air-sea carbon exchange.

In much of the SO, the supply of iron and availability of light are key mediators of primary productivity [*Boyd*, 2002; *Fauchereau et al.*, 2011]. During summer when sunlight is abundant, primary productivity is mainly limited by iron, which is depleted in the surface ocean and enriched at depth [*Venables and Moore*, 2010; *Boyd and Ellwood*, 2010]. In such conditions, introduction of iron-rich subsurface water through vertical mixing can enhance the primary productivity and increase CHL [*Carranza and Gille*, 2015]. In contrast, during the winter, deep convective mixing supplies iron to the upper ocean [*Tagliabue et al.*, 2014], but simultaneously decreases mixed-layer-average light levels for photosynthesis [*Nelson and Smith*, 1991]. *Fauchereau et al.* [2011] found large spatial and seasonal variability in the correlation between CHL and MLD, and propose vertical mixing as an important driver for the surface CHL perturbation through changes in limitation by either iron or light.

If the mesoscale modulation of MLD has a significant impact, we can anticipate that deeper vertical mixing in anticyclones would supply iron-rich subsurface water more than cyclones in summer but decreases light level further in winter when compared with cyclones. Then the footprint of mesoscale modulation of MLD on CHL would appear as a seasonal cycle in $\rho_{SSH',CHL'}$. This raises the question, do satellite observations of SSH and CHL reveal such a signal? In this study, motivated by the systematic modulation of MLD by the mesoscale and its link to factors limiting productivity, we examine $\rho_{SSH',CHL'}$ at the mesoscale in the SO where the mean eddy scale is between 75 km to 100 km [*Chelton et al.*, 2011b]. We utilize satellite observations and an eddy-rich biogeochemical numerical model to better understand the physical and biological interactions in the mesoscale.

After briefly describing the observations and physical-biogeochemical model, we first report on observed $\rho_{SSH',CHL'}$ in the SO, particularly along the Antarctic Circumpolar Current (ACC). We then evaluate the influences of MLD modulation by mesoscale dynamics on the observed correlation by utilizing a numerical model.

2. Satellite data and an eddy-rich physical-biogeochemical model

The procedure to obtain the anomaly of SSH and CHL starts from preparing weekly mean fields from 1998 to 2007. The weekly mean SSH field was prepared by averaging the daily absolute dynamic topography mapped on the 1/4×1/4 degree grid by Collecte Localis Satellites / Archiving, Validation and Interpretation of Satellite Oceanographic data (CLS/AVISO). This data set does not contain mesoscale variability whose length scale is smaller than 0.4 degree [*Chelton et al.*, 2011b]. The processes to obtain the weekly CHL include mapping log-transformed daily CHL estimation from Sea-Viewing Wide Field-of-View Sensor (SeaWiFS) on the same grid as SSH anomalies, applying loess smoother in time and transforming back to its original linear scale [*Gaube et al.*, 2013]. The weekly average attenuates the features whose time scale is shorter than a few days (e.g., submesoscale features). Then the anomalies of SSH and CHL were estimated by spatially high-pass filtering the weekly data with 6 degree half-power cutoff which retains the variability with wavelength scale shorter than 6 degree. Details of the processing are provided in Supporting Information.

We evaluate the role of mesoscale phenomena by considering SSH anomalies exceeding 5 cm in absolute value. Such deviations in SSH include those driven by not only coherent eddy structures expressed by closed contours of anomalies [*Chelton et al.*, 2011b] but also

other mesoscale flow features (e.g., fronts). Positive SSH anomalies represent anticyclones while negative anomalies corresponds to cyclones for coherent eddy structures. In case of fronts, a positive/negative SSH anomaly is likely to be found on the less/more dense side of the front in the SO where the sea level increases toward the equator. When identified from a few weekly maps of SSH anomaly using the same eddy detection algorithm as the one in *Chelton et al.* [2011b], coherent eddy structures account for approximately 67% of SSH anomalies with the size greater than 5 cm. For simplicity, positive/negative SSH anomalies are referred to anticyclones/cyclones in this study, recognizing that the underlying phenomenology is more complicated.

A simulation of eddy-rich coupled physical and biogeochemical states is provided by a Biogeochemical Elemental Cycling (BEC) model [*Moore et al.*, 2002, 2004, 2013] embedded in the 1/10 degree resolution ocean circulation component of the Community Earth System Model (CESM). Phytoplankton growth is regulated by both light and nutrients (iron in this regime) as described in Equation 1 of the Supporting Information. Vertical mixing is represented by the K-Profile Parameterization (KPP) scheme [*Large et al.*, 1994], in which diapycnal diffusivity is set proportional to the vertical mixing depth. We use the vertical mixing depth as a measure of MLD because the vertical mixing of tracers such as nutrients is subject to it. Although the vertical mixing depth is generally shallower than the mixed-layer depth determined by potential density criteria in the model simulation, they show a strong correlation (correlation coefficient > 0.8 with p-value < 0.01). Hence it is reasonable to expect that the vertical mixing depth (or MLD hereafter) is modu-

lated by the mesoscale in a manner similar to that of the mixed-layer depth. A detailed description of the model can be found in Supporting Information.

3. Seasonal correlation between anomalies of sea surface height and chlorophyll

Our analysis of satellite observations of CHL and SSH anomalies reveals a positive $\rho_{SSH',CHL'}$ along the ACC in summer (January–March, Figure a) and a negative $\rho_{SSH',CHL'}$ in winter (July–September, Figure b) [e.g., *Frenger*, 2013]. In winter, the signal is not as clear as in the summer, which may be due to the lower CHL variability. The condition of low sun elevation, sun glint and frequent storm system passages lowers the observational density of satellite CHL data in winter. Lower density can be problematic in computing the anomalies with respect to the spatial mean and possibly obscure the correlation signal. The seasonality of the correlation along the ACC is clearly different from that to the north of it where the correlation is generally negative all year long.

To identify the mechanisms by which mesoscale processes in the ACC influence CHL, we examine the solution of an eddy-rich physical-biogeochemical model. The 5-day mean model fields are first mapped on the same 1/4 degree grid as the satellite data using bilinear interpolation to suppress the impact from features that the satellite observations cannot represent. Encouragingly, the simulation largely reproduces the observed seasonality in $\rho_{SSH',CHL'}$ (Figure c-d), as well as SSH variability, mean and seasonality of near-surface CHL and seasonal variability in the depth of mixed layer (Figures S1-S2 in Supporting Information). There are broad areas of strongly positive $\rho_{SSH',CHL'}$ along the ACC and at its southern margins in summer, changing sign in winter, especially in the Indian

and Pacific Ocean sectors. South of the ACC, correlations are noisier and observed and modeled correlations agree less, perhaps due to processes that are missing in the model, such as iron supply from melting sea ice, or possibly weaker observational constraints in the polar zone.

We examined $\rho_{SSH',CHL'}$ averaged zonally along the path of the ACC (defined by SSH isolines between -80 cm and -20 cm, see Supporting Information) to draw out seasonal patterns. Correlations are positive within the ACC from summer to fall (January–June), then switch to negative until early spring (October) (Figure 2a). Observations indicate that the seasonality in the correlation is lagged south of the regions with -50 cm SSH; the model, however, shows a more consistent phasing over the meridional extent of the ACC region (Figure 2b). In spite of this inconsistency, the simulation captures the major correlations in the ACC, justifying an examination of the simulation to identify the underlying mechanisms generating observed variability in mesoscale modulations of the CHL field.

4. Mechanisms in an eddy-rich biogeochemical model

We hypothesize that oceanic mesoscale dynamics play an important role in the seasonality of $\rho_{SSH',CHL'}$ along the ACC by regulating the availability of light and iron, resulting in differing CHL responses in summer and winter. There is a positive correlation between MLD and SSH anomalies in all seasons over most of the SO in the model, suggesting that anticyclones have deeper mixed layers than cyclones (Figures e,f and 2e). This MLD modulation by the mesoscale is more intense and systematic in winter than in summer, evident in a larger MLD difference between anticyclones and cyclones (Figure 3a,b) and a higher correlation coefficient between anomalies of SSH and MLD (Figure 2e). The de-

gree of mesoscale MLD modulation increases with the amplitude of the SSH anomaly. For example, the wintertime MLD difference between positive and negative SSH anomalies whose amplitudes are greater than 5 cm is 24 m; this statistically significant difference increases to 55 m when the amplitude of SSH anomalies greater than 20 cm are considered. The simulated correlation between SSH anomalies and MLD (Figure 2e), seasonality in mesoscale MLD modulation and dependency of MLD anomaly on the SSH anomaly amplitude are consistent with observed variations of MLD in eddies, whereby anticyclones exhibit weaker stratification and deeper mixed layers than cyclones [*Hausmann et al.*, 2017].

In winter, light is the primary factor limiting productivity throughout the whole water column and iron limitation is of diminished importance (Figure 3b). Since light is supplied at the surface and attenuates with depth, simulated mixed-layer mean light (or photosynthetically active radiation; $\langle \mathrm{PAR} \rangle$) declines with increasing MLD. We find that anomalies of $\langle \mathrm{PAR} \rangle$ estimated from the model are negatively correlated with SSH anomalies throughout the year (Figure 2d). $\langle \mathrm{PAR} \rangle$ is approximately 30% lower in anticyclones than cyclones in winter (Figure 4a) and about 7% lower in summer (Figure 4c), suggesting deeper mixing in anticyclones decreases $\langle \mathrm{PAR} \rangle$ experienced by phytoplankton in the mixed layer. Thus deeper vertical mixing in anticyclones has the potential to limit productivity in winter, resulting in lower CHL in anticyclones versus cyclones (Figure 3a,d). This argument is supported by the $\rho_{SSH',CHL'}$ along the ACC in the Pacific and Indian Ocean sectors, although it is less clear in the Atlantic Ocean sector (Figure (b,d)). The Atlantic Ocean sector exhibits the shallowest mixed layers in winter that relieve the light limitation

for the phytoplankton growth, leading to a less distinct relationship between anomalous vertical mixing and CHL. The Pacific and Indian Ocean sectors, however, have deeper mixed layers and clearer negative $\rho_{SSH',CHL'}$ along the ACC in both the observations and the model than the Atlantic Ocean sector.

In contrast, productivity is iron limited in the summer (Figure 3a). The model simulation shows that anticyclones in the ACC have approximately 15% more iron averaged over the mixed layer ($\langle \mathrm{Fe} \rangle$) in summer (Figure 4c) than cyclones, which promotes higher productivity and CHL. The $\langle \mathrm{Fe} \rangle$ anomaly is larger in winter than in summer (30% v.s. 15%, Figure 4a,c), which suggests the link between the intensity of mesoscale MLD modulation and iron supply. However, the positive $\langle \mathrm{Fe} \rangle$ anomaly associated with anticyclones in winter does not lead to enhanced productivity under the light-limited environment. Iron concentrations are elevated both within and below the mixed layer (Figure 3a-c), suggesting that part of the enhanced vertical flux in anticyclones is attributable to a larger iron reservoir underlying these features at depth. Without anomalous deep mixing, the positive $\langle \mathrm{Fe} \rangle$ anomaly in anticyclones cannot be maintained under the active consumption of iron by phytoplankton.

A budget analysis for $\langle \mathrm{Fe} \rangle$ along the ACC (Figure 4b,d; see Supporting Information for details) quantifies the various mechanisms of iron supply and removal. We only consider areas where bathymetry is deeper than 200 m in order to avoid the direct influence from shelf regions [*Carranza et al.*, 2017]. Iron is supplied to the mixed layer by lateral and vertical advection, vertical mixing, aeolian input of dust, and entrainment associated with changes in the MLD; it is removed through the biogeochemical sink term, which represents

phytoplankton uptake and scavenging on sinking particulates. Among these processes, we find that the supply of iron by vertical mixing differs most between anticyclones and cyclones. Supply of iron by vertical mixing in anticyclones has a median value that is roughly 10% higher than in cyclones when normalized by the median ⟨Fe⟩ in the ACC. The contributions from lateral and vertical advection tend to cancel each other, reducing the contribution as a whole, and the difference in median value of the total advection between anticyclones and cyclones is less than 1%. The differences in other terms are also small (less than 2%) compared to that in the vertical mixing. Iron input from dust increases ⟨Fe⟩ but, as might be expected, the differences between anticyclones and cyclones are negligible. The biogeochemical sink is the largest in summer with slightly more loss of iron in anticyclones due to higher phytoplankton productivity. The entrainment term shows little contribution after being normalized by the MLD, and differences between anticyclones and cyclones are negligible; thus it is not plotted in Figure 4b,d.

Supply of iron through vertical mixing is controlled by both the MLD and the vertical gradient of iron, suggesting that knowing the vertical structure of iron is important to understand the enhanced vertical mixing term in anticyclones, especially in summer when the MLD differences between anticyclones and cyclones are relatively small. The model simulation suggests that anticyclones have an enhanced vertical iron gradient relative to cyclones in summer. The iron limiting factor shows a smaller difference between cyclones and anticyclones at the surface than at 50 m (the solid line in Figure 3c), suggesting that anticyclones have more favorable conditions for the enhanced iron supply by vertical mixing than cyclones. Combined with the fact that both the observations [*Hausmann*

et al., 2017] and the model simulation (Figure 3a,b) suggest that MLD modulation by the mesoscale is relatively subtle in summer, the enhanced vertical iron gradient in anticyclones may be the key feature driving differences in iron supply by vertical mixing—as opposed to changes in the depth of mixed layer.

5. Discussion

Our study emphasizes the importance of mesoscale processes affecting phytoplankton growth through MLD changes impacting iron and light availability. Features with anomalously high SSH (anticyclones) are characterized by deeper mixed layers while those with negative SSH anomalies (cyclones) have anomalously shallow MLDs. These modulations of the MLD affect light levels resulting in lower CHL in anticyclones, and higher CHL in cyclones in winter. The MLD modulation by the mesoscale is also seen in summer, and the median MLD difference is statistically significant but small: less than 5 m along the ACC. Nevertheless, deeper MLDs and larger vertical gradients of iron together make iron supply by vertical mixing greater in anticyclones than cyclones, and contribute to iron anomalies in the mixed layer in all seasons. Our results suggest that anomalies in iron availability and light exposure associated with the mesoscale and the alternating role of iron and light limitation in summer and winter play a major role in explaining the seasonally changing $\rho_{SSH',CHL'}$ along the ACC (Figure 3e,f).

The eddy-rich biogeochemical model generates higher levels of iron in anticyclones along the ACC in both seasons. A possible explanation for higher iron in anticyclones in summer is preconditioning during winter. In winter when the MLD modulation by the mesoscale is particularly intense, deeper mixed layers in anticyclones have considerably higher iron

concentration than the shallower mixed layers of cyclones. Anomalously high iron in anticyclones in winter is not heavily used due to the lack of sunlight, and subsequently may promote elevated primary productivity in summer. The mixed layer shoals rapidly after winter, and iron in the mixed layer is consumed by primary producers, creating vertical gradients of iron. Then vertical mixing at the base of the mixed layer continues to entrain iron from the layer that was previously in the mixed layer during winter. Hence anticyclones have relatively iron-enriched water below the summertime mixed layer compared to cyclones (Figure 3a), and this may contribute to differences in iron limitation among the two types of features. This explanation can be applied to well-formed and long-lived eddies whose lifespans are of the order of months. Given that many eddies along the ACC survive three months and longer [*Frenger et al.*, 2015], the preconditioning explanation is plausible.

In other highly dynamic regions of intense eddy activity such as the Gulf Stream and the Kuroshio Current, it is thought that eddies cause anomalies of CHL concentration primarily through eddy-driven advection of large-scale CHL gradients, i.e. stirring and trapping [*Kouketsu et al.*, 2015; *Gaube et al.*, 2014]. The lateral gradient of CHL suggests that advective mechanisms cannot be entirely ruled out in understanding the correlations along the ACC (Figure S1c-d in Supporting Information). However, the lateral gradient in CHL is not as strong as in either the Gulf Stream or the Kuroshio Current, owing to light limitation in the winter and iron limitation in the summer (the so-called "High Nitrate Low Chlorophyll" (HNLC) condition).

Understanding the influence of mesoscale processes on vertical mixing and iron supply is important for more accurate estimation of SO's role in global carbon cycle. However, coarse resolution climate modeling systems on which many studies rely do not resolve the ocean's mesoscale. Such models cannot capture mixed layer modulation by the mesoscale, leading to as yet unknown biases in air-sea carbon dioxide flux. Quantifying the integrated effects of these phenomena on biological uptake and the supply of carbon rich water from depth is necessary to better understand the role of the mesoscale in biogeochemical cycling in the SO.

Acknowledgments. The altimeter products were produced and distributed by AVISO (http://www.aviso.altimetry.fr/), as part of the Ssalto ground processing segment. The CHL observations are available through NASA MEaSUREs Ocean Color Product Evaluation Project (ftp://ftp.oceancolor.ucsb.edu/). The observational data for the depth of the mixed-layer is from *Dong et al.* [2008] and for iron concentration is from *Tagliabue et al.* [2014]. Computational facilities have been provided by the Climate Simulation Laboratory, which is managed by CISL at NCAR. NCAR is supported by the National Science Foundation. The CESM source code is freely available at http://www2.cesm.ucar.edu. The analysis code for the Fe budget averaged over the mixed layer is available at https://github.com/hajsong/tracerbudget. HS, JM and DJM were supported by the NSF MOBY project (OCE-1048926). DJM also acknowledges support from NSF (OCE-1048897) and NASA (NNX13AE47G). In addition, PG acknowledges support from NSF (OCE-1558809) and NASA (NNX13AE47G, NNX16AH9G).

References

Boyd, P. W. (2002), The role of iron in the biogeochemistry of the Southern Ocean and equatorial Pacific: a comparison of in situ iron enrichments, *Deep-Sea Res., Pt II*, *49*(9–10), 1803–1821, doi:http://dx.doi.org/10.1016/S0967-0645(02)00013-9.

Boyd, P. W., and M. J. Ellwood (2010), The biogeochemical cycle of iron in the ocean, *Nature Geoscience*, *3*(10), 675–682.

Bowie, A., D. Whitworth, E. Achterberg, R. Mantoura, and P. Worsfold (2002), Biogeochemistry of Fe and other trace elements (Al, Co, Ni) in the upper Atlantic Ocean, *Deep-Sea Res. Pt I*, *49*(4), 605–636.

Campbell, J. W. (1995), The lognormal distribution as a model for bio-optical variability in the sea, *J. Geophys. Res.*, *100*(C7), 13,237–13,254, doi:10.1029/95JC00458.

Carranza, M., S. Gille, A. Piola, M. Charo, and S. Romero (2017), Wind modulation of upwelling a the shelf-break front off patagonia: Observational evidence, *J. Geophys. Res. Oceans*, *122*, 2401–2421.

Carranza, M. M., and S. T. Gille (2015), Southern Ocean wind-driven entrainment enhances satellite chlorophyll-a through the summer, *J. Geophys. Res. Oceans*, *120*(1), 304–323.

Chelton, D. B., and M. G. Schlax (2003), The accuracies of smoothed sea surface height fields constructed from tandem satellite altimeter datasets, *J. Atmos. Oceanic Technol.*, *20*, 1276–1302.

Chelton, D. B., M. G. Schlax, R. M. Samelson, and R. A. de Szoeke (2007), Global observations of large oceanic eddies, *Geophys. Res. Lett.*, *34*, L15,606.

Chelton, D. B., P. Gaube, M. G. Schlax, J. J. Early, and R. M. Samelson (2011a), The Influence of Nonlinear Mesoscale Eddies on Near-Surface Oceanic Chlorophyll, *Science*, *334*(6054), 328–332.

Chelton, D. B., M. G. Schlax, and R. M. Samelson (2011b), Global observations of nonlinear mesoscale eddies, *Prog. Oceanogr.*, *91*(2), 167–216, doi: http://dx.doi.org/10.1016/j.pocean.2011.01.002.

Clayton, S., S. Dutkiewicz, O. Jahn, C. Hill, P. Heimbach, and M. J. Follows (2016), Biogeochemical versus ecological consequences of modeled ocean physics, *Biogeosciences Discussions*, *2016*, 1–20, doi:10.5194/bg-2016-337.

Dong, S., J. Sprintall, S. T. Gille, and L. Talley (2008), Southern Ocean mixed-layer depth from Argo float profiles, *J. Geophys. Res.*, *113*, C06,013.

Dufois, F., N. J. Hardman-Mountford, J. Greenwood, A. J. Richardson, M. Feng, S. Herbette, and R. Matear (2014), Impact of eddies on surfacechlorophyll in the South Indian Ocean, *J. Geophys. Res. Oceans*, *119*, 8061–8077, doi:10.1002/2014JC010164.

Dufois, F., N. J. Hardman-Mountford, J. Greenwood, A. J. Richardson, M. Feng, and R. J. Matear (2016), Anticyclonic eddies are more productive than cyclonic eddies in subtropical gyres because of winter mixing, *Science Advances*, *2*(5), e1600,282–e1600,282.

Fauchereau, N., A. Tagliabue, L. Bopp, and P. M. S. Monteiro (2011), The response of phytoplankton biomass to transient mixing events in the Southern Ocean, *Geophys. Res. Lett.*, *38*, L17,601, doi:10.1029/ 2011GL048498.

Ferrari, R., and C. Wunsch (2009), Ocean circulation kinetic energy: Reservoirs, sources, and sinks, *Annu. Rev. Fluid Mech.*, *41*, 253–282, doi:

10.1146/annurev.fluid.40.111406.102139.

Frenger, I. (2013), On Southern Ocean eddies and their impacts on biology and the atmosphere, Ph.D. thesis, ETH Zurich, Zurich, Switzerland, doi:10.3929/ethz-a-009938120.

Frenger, I., M. Münnich, N. Gruber, and R. Knutti (2015), Southern ocean eddy phenomenology, *Journal of Geophysical Research: Oceans*, *120*(11), 7413–7449, doi:10.1002/2015JC011047.

Garver, S. A., and D. A. Siegel (1997), Inherent optical property inversion of ocean color spectra and its biogeochemical interpretation: 1. time series from the sargasso sea, *J. Geophys. Res. Oceans*, *102*(C8), 18,607–18,625, doi:10.1029/96JC03243.

Gaube, P., D. B. Chelton, P. G. Strutton, and M. J. Behrenfeld (2013), Satellite observations of chlorophyll, phytoplankton biomass, and ekman pumping in nonlinear mesoscale eddies, *J. Geophys. Res. Oceans*, *118*, 6349–6370, doi:10.1002/2013JC009027.

Gaube, P., D. J. McGillicuddy, Jr., D. B. Chelton, M. J. Behrenfeld, and P. G. Strutton (2014), Regional variations in the influence of mesoscale eddies on near-surface chlorophyll, *J. Geophys. Res. Oceans*, *119*, doi:10.1002/2014JC010111.

Geider, R., H. MacIntyre, and T. Kana (1998), A dynamic regulatory model of phytoplankton acclimation to light, nutrients, and temperature, *Limnol. Oceanogr.*, *43*, 679–694.

Hausmann, U., D. J. McGillicuddy, Jr., and J. Marshall (2017), Observed mesoscale eddy signatures in Southern Ocean surface mixed-layer depth, *J. Geophys. Res. Oceans*, *122*, 617–635, doi:10.1002/ 2016JC012225.

Kouketsu, S., H. Kaneko, T. Okunishi, K. Sasaoka, S. Itoh, R. Inoue, and H. Ueno (2015), Mesoscale eddy effects on temporal variability of surface chlorophyll a in the Kuroshio Extension, *J. of Oceanogr.*, *72*(3), 439–451.

Large, W., J. McWilliams, and S. Doney (1994), Oceanic vertical mixing: A review and a model with nonlocal boundary layer parameterization, *Rev. Geophys.*, *32*, 363–403.

Maritorena, S., D. A. Siegel, and A. R. Peterson (2002), Optimization of a semianalytical ocean color model for global-scale applications, *Appl. Opt.*, *41*(15), 2705–2714, doi: 10.1364/AO.41.002705.

Mawji, E., et al. (2015), The GEOTRACES intermediate data product 2014, *Mar. Chem.*, *177*, 1–8, doi:https://doi.org/10.1016/j.marchem.2015.04.005.

McGillicuddy, D. J., Jr. (2016), Mechanisms of Physical-Biological-Biogeochemical Interaction at the Oceanic Mesoscale, *Annu. Rev. Mar. Sci.*, *8*(1), 125–159.

McGillicuddy, D. J., Jr., L. A. Anderson, N. R. Bates, T. Bibby, K. Buesseler, C. Carlson, C. Davis, C. Ewart, P. Falkowski, S. Goldthwait, D. Hansell, W. Jenkins, R. Johnson, V. Kosnyrev, J. Ledwell, Q. Li, D. Siegel, and D. Steinberg (2007), Eddy/wind interactions stimulate extraordinary mid-ocean plankton blooms, *Science*, *316*, 1021–1026.

Moore, J. K., S. C. Doney, J. A. Kleypas, D. M. Glover, and I. Y. Fung (2002), An intermediate complexity marine ecosystem model for the global domain, *Deep Sea Res., Part II*, *49*(1-3), 403–462.

Moore, J. K., S. C. Doney, and K. Lindsay (2004), Upper ocean ecosystem dynamics and iron cycling in a global three-dimensional model, *Global Biogeochem. Cycles*, *18*, GB4028, doi:10.1029/2004GB002220.

Moore, J. K., K. Lindsay, S. C. Doney, M. C. Long, and K. Misumi (2013), Marine ecosystem dynamics and biogeochemical cycling in the Community Earth System Model [CESM1(BGC)]: Comparison of the 1990s with the 2090s under the RCP4.5 and RCP8.5 scenarios, *J. Clim.*, *26*(23), 9291–9312, doi:10.1175/JCLI-D-12-00566.1.

Morel, A., and S. Maritorena (2001), Bio-optical properties of oceanic waters: a reappraisal, *J. Geophys. Res.*, *106*(C4), 7163–7180, doi:10.1029/2000jc000319.

Nelson, D. M., and W. O. Smith, Jr. (1991), Sverdrup revisited: Critical depths, maximum chlorophyll levels, and the control of Southern Ocean productivity by the irradiance-mixing regime, *Limnology and Oceanography*, *36*(8), 1650–1661.

Robinson, A. R. (Ed.) (1983), *Eddies in Marine Science*, Springer Berlin Heidelberg, doi:10.1007/978-3-642-69003-7.

Rodríguez, J., J. Tintoré, J. T. Allen, J. M. Blanco, D. Gomis, A. Reul, J. Ruiz, V. Rodríguez, F. Echevarría, and F. Jiménez-Gómez (2001), Mesoscale vertical motion and the size structure of phytoplankton in the ocean, *Nature*, *410*(6826), 360–363.

Siegel, D. A., S. Maritorena, N. B. Nelson, D. A. Hansell, and M. Lorenzi-Kayser (2002), Global distribution and dynamics of colored dissolved and detrital organic materials, *J. Geophys. Res. Oceans*, *107*(C12), 21–1–21–14, doi:10.1029/2001JC000965.

Tagliabue, A., T. Mtshali, O. Aumont, A. Bowie, M. Klunder, A. Roychoudhury, and S. Swart (2012), A global compilation of dissolved iron measurements: focus on distributions and processes in the Southern Ocean, *Biogeosciences*, *9*, 2333–2349, doi:10.5194/bg-9-2333-2012.

Tagliabue, A., J.-B. Sallée, A. R. Bowie, M. Lévy, S. Swart, and P. W. Boyd (2014), Surface-water iron supplies in the Southern Ocean sustained by deep winter mixing, *Nature Geoscience*, *7*, 314–320, doi:10.1038/ngeo2101.

Venables, H., and C. Moore (2010), Phytoplankton and light limitation in the Southern Ocean: Learning from high-nutrient, high-chlorophyll areas, *J. Geophys. Res.*, *115*, C02,015, doi:10.1029/2009JC005361.

Whitt, D. B., J. R. Taylor, and M. Lévy (2017a), Synoptic-to-planetary scale wind variability enhances phytoplankton biomass at ocean fronts, *J. Geophys. Res. Oceans*, *122*, 4602–4633.

Whitt, D. B., M. Lévy, and J. R. Taylor (2017b), Low- and high-frequency oscillatory winds synergistically enhance nutrient entrainment and phytoplankton at fronts, *J. Geophys. Res. Oceans*, *122*, doi:10.1002/2016JC012400.

Wunsch, C. (1999), Where do ocean eddy heat fluxes matter?, *J. Geophys. Res.*, *104*, 13,235–13,249.

Xu, C., X.-D. Shang, and R. X. Huang (2014), Horizontal eddy energy flux in the world oceans diagnosed from altimetry data, *Scientific Reports*, *4*, 5316, doi:10.1038/srep05316.

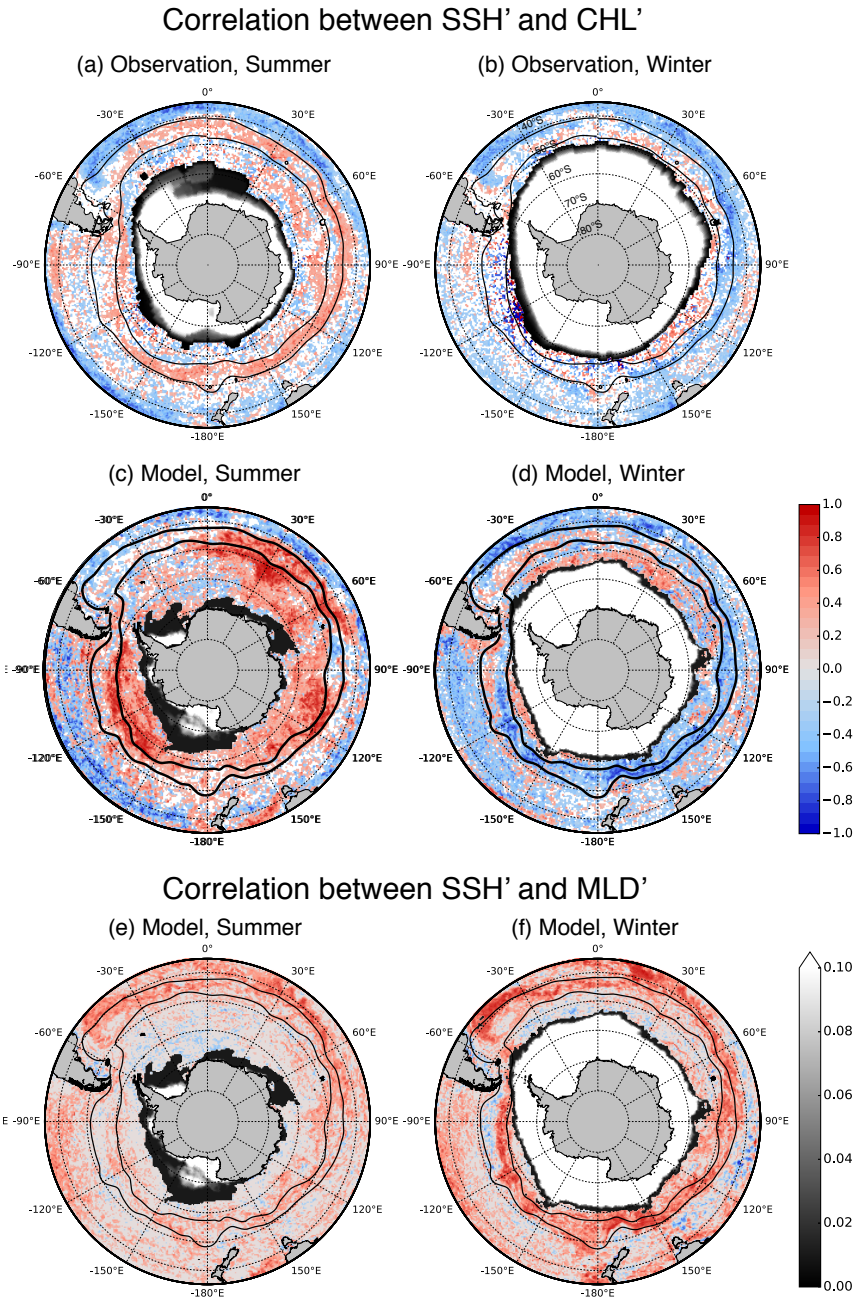

Figure 1. The correlation coefficients between anomalies of SSH and CHL in the (a,b) satellite observations and (c,d) 1/10 degree ocean model are shown as pseudo-color images. The left and right columns show the (a,c) correlation for austral summer (January-March) and (b,d) austral winter (July-September), respectively. Black contours mark the sea level isolines of −20 cm and −80 cm that enclose the ACC. The masks in gray scale around Antarctica represent the sea-ice area fraction from the Hadley Centre Sea Ice and Sea Surface Temperature data set in (a,b) and from the model in (c,d). The sea-ice areas are masked by the color changing from white to black. The correlation coefficients between anomalies of SSH and MLD in the eddy-rich model are also presented similarly in (e,f). The areas in white have either a correlation coefficient close to zero or a P-value greater than 0.01 (statistically insignificant).

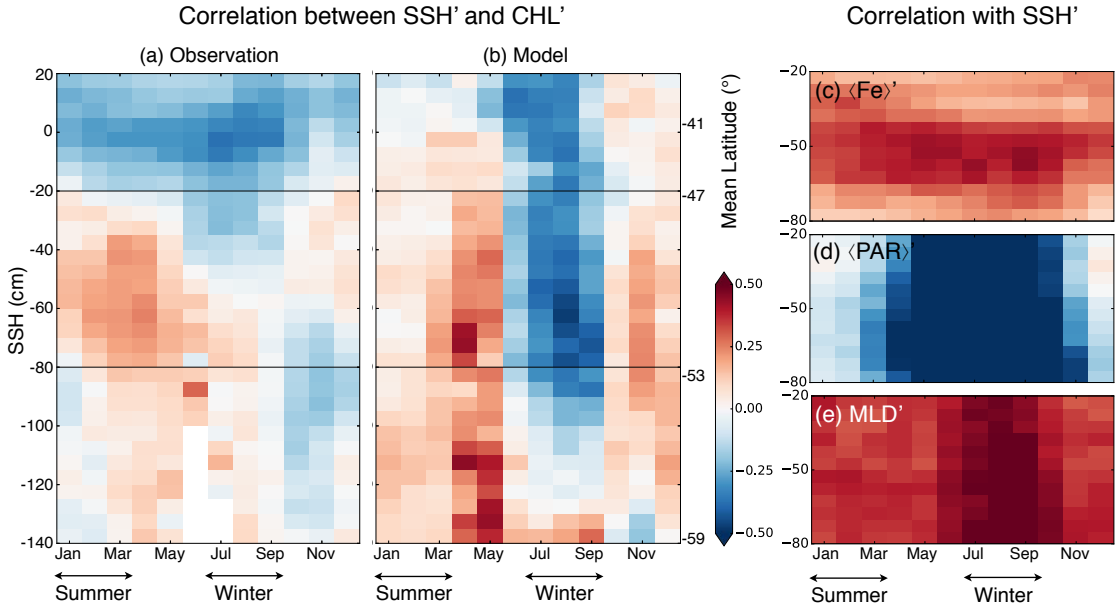

Figure 2. The correlation of anomalies in SSH and CHL along SSH isolines in (a) observations and (b) model. The areas within two black lines at -80 cm and -20 cm approximate the ACC and correspond to the black contours in Figure 1. The equivalent latitude is shown on the right y-axis in (b). Panels on the right are the correlation coefficients of anomalies of the (c) iron and (d) light limiting factor averaged over the MLD, and (e) MLD with SSH anomalies from the model. Correlations are statistically significant at the 99% confidence level.

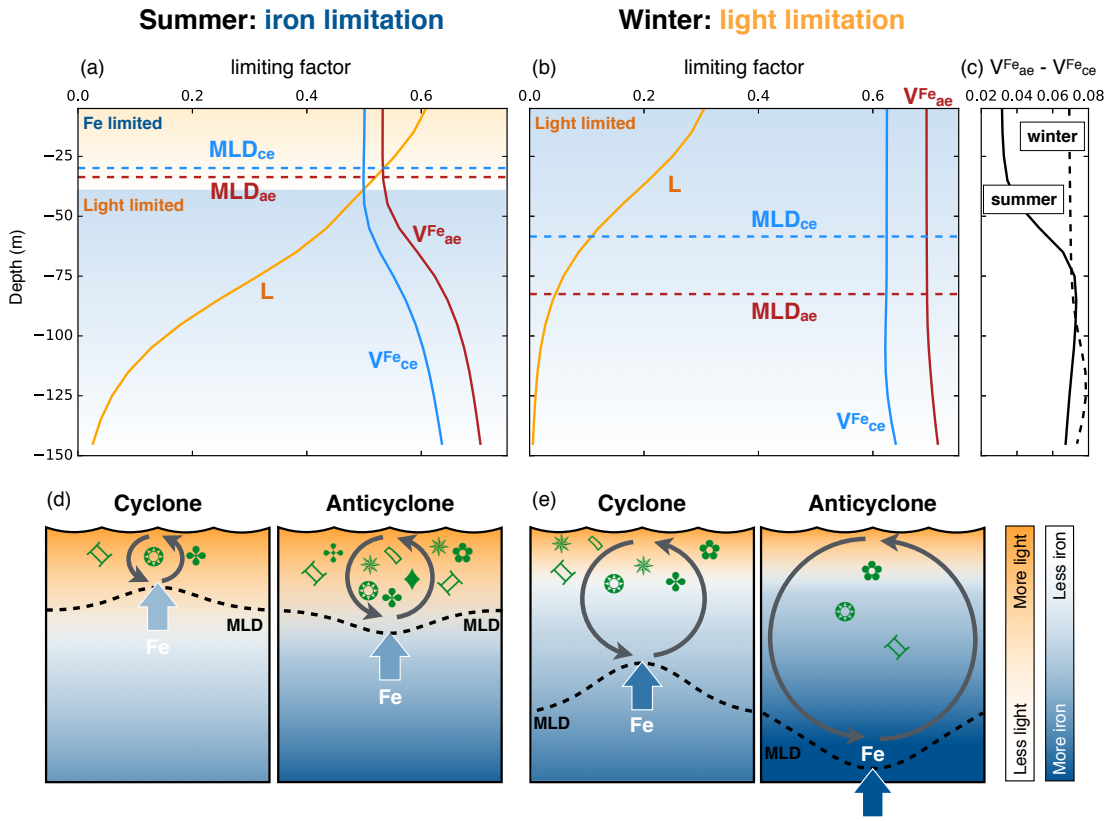

Figure 3. (a,b) The median vertical profiles of light limiting factor (L) and iron limiting factors ($V^{\mathrm{Fe}} = \mathrm{Fe}/(\mathrm{Fe} + K_{\mathrm{Fe}})$) for anticyclones ($V^{\mathrm{Fe}}{}_{ae}$) and cyclones ($V^{\mathrm{Fe}}{}_{ce}$) in the biogeochemical model (Supporting Information, Equation 1) averaged in the ACC. In summer, iron is the limiting factor for the primary productivity within the mixed layer (a). The magnitude of limiting factor is inversely related to its' effect on primary productivity, e.g., light is more important than iron concentration throughout the whole water column in winter (b). Blue and red dotted lines represent the median value for MLD within cyclones and anticyclones, respectively, in the ACC. Panel (c) displays the vertical profile of the iron limiting factor differences ($V^{\mathrm{Fe}}{}_{ae} - V^{\mathrm{Fe}}{}_{ce}$) in summer (solid line) and winter (dashed line). Confidence intervals of the MLDs are omitted in (a-c) because they are too narrow. A diagram depicting the mesoscale modulation of MLD and its impact on phytoplankton biomass in two different seasons in the SO are shown in panels (d) and (e). The brightness of the blue and orange shading represents the iron concentration and sunlight intensity, respectively. In summer, primary production is controlled by iron supply (blue arrows) and not light in the mixed layer (d). In winter, intensive vertical mixing enriches iron concentration near the surface, but low light availability limits primary production (e).

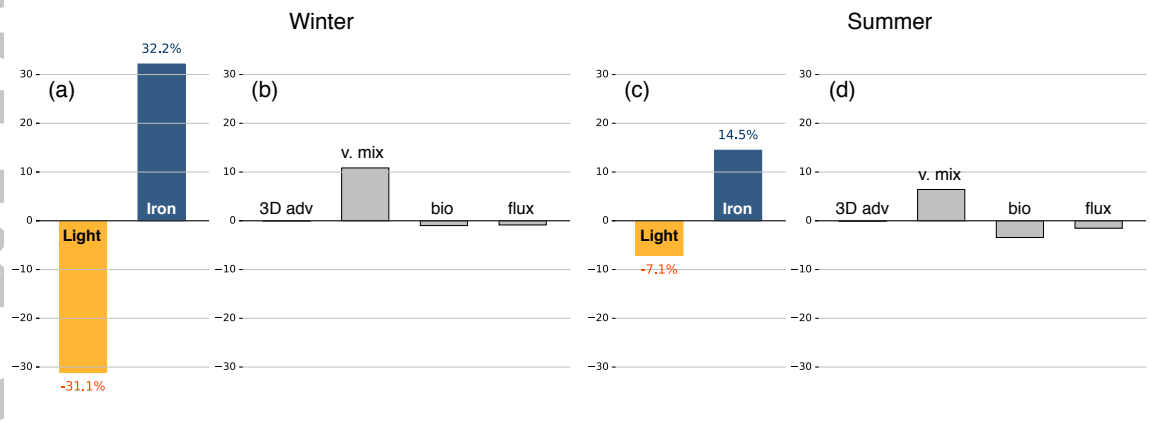

Figure 4. The bar plots in (a,c) represent the percentage differences in light level (yellow) and iron concentration (blue) in the mixed layer between anticyclones and cyclones in winter and summer, respectively. The percentage differences between anticyclones and cyclones in various contribution to the iron averaged over the mixed layer are plotted in (b,d). Those contributions are 3-dimensional advection (3D adv including both buoyancy- and wind-driven transports), vertical mixing (v. mix), biogeochemical cycle (bio) and flux from dust (flux), and they are normalized by the averaged iron in the mixed layer. The contribution from entrainment is little and not plotted. The 95% confidence intervals estimated using bootstrapping are narrow and not shown.